

Superhydrophobic polycarbosilane membranes for purification of solar hydrogen

Miwako Kubo ^a, Kohei Okibayashi ^a, Misako Kojima ^a, Ryota Mano ^a, Yusuke Daiko ^a, Sawao Honda ^a, Samuel Bernard ^b, Yuji Iwamoto ^{a,*}

^a Department of Life Science and Applied Chemistry, Graduate School of Engineering, Nagoya Institute of Technology, Gokiso-cho, Showa-ku, Nagoya 466-8555, Japan

^b Univ. Limoges, CNRS, IRCER, UMR 7315, F-87000 Limoges, France

ARTICLE INFO

Keywords:

Polycarbosilanes (PCSs)
Hydrophobic SiCH organic-inorganic hybrid
Hydrogen-selective membrane
Preferential hydrogen permeation
Permeate H₂O-induced plugging

ABSTRACT

Superhydrophobic membranes composed of an organic-inorganic hybrid polymer, namely polycarbosilane (PCS) with Mw of $4\text{--}8.9 \times 10^3$, were formed on a mesoporous $\gamma\text{-Al}_2\text{O}_3$ -modified $\alpha\text{-Al}_2\text{O}_3$ porous support. Under dry condition at 50 °C, the supported PCS membranes exhibited H₂ permeance of $1.1\text{--}1.6 \times 10^{-6} \text{ mol}\cdot\text{m}^{-2}\cdot\text{s}^{-1}\cdot\text{Pa}^{-1}$ and H₂/N₂ selectivity of 9.7–12.6 together with unique H₂/He selectivity of 1.4–1.6. Even under saturated humidity at 50 °C, H₂ permeance remained at $7.7 \times 10^{-8} \text{ mol}^{-1} \text{ m}^{-2} \text{ s}^{-1} \text{ Pa}^{-1}$ with improved H₂/N₂ selectivity of 26. Moreover, when the measurements were performed using a H₂-N₂ (2:1) mixed feed gas as a simulated syngas produced by novel solar hydrogen production systems, the H₂ permeance almost unchanged, while the N₂ permeance was below the limit of detection. These results revealed a great potential of PCSs to develop novel H₂-selective membranes for purifying solar hydrogen under high-humidity conditions around 50 °C. Further study on the gas permeation behaviors of He, H₂ and N₂ suggested that the enhanced H₂/N₂ selectivity under the high-humidity conditions could be explained by the synergistic effect of preferential H₂ permeation through the dense PCS network governed by the solid state diffusion mechanism and blockage of N₂ permeation through micropore channels within the PCS network by the permeate H₂O-induced plugging at around the hetero interface between the superhydrophobic PCS and highly hydrophilic $\gamma\text{-Al}_2\text{O}_3$.

1. Introduction

Because of its high potential to replace the current hydrogen production by the steam reforming of naphtha and methane, photoelectrochemical (PEC) water-splitting [1–3] has received much attention as an environmental-friendly hydrogen production method. However, due to its co-production of gaseous hydrogen (H₂) and oxygen (O₂) which explosively react in a wide range (4–95%) of H₂ concentration [4], H₂ gas must be immediately separated from the syngas under the high-humidity conditions at low temperatures around 50 °C [5].

Membrane separation is attractive as one of the low-cost H₂ gas purification technologies. However, under the required H₂ gas separation conditions, there are technical issues such as water-induced swelling for polymer membranes and lower H₂ permeance for metal [6], polymer [7] and supported liquid membranes [8]. Microporous amorphous silica (SiO₂) membranes exhibit a higher H₂-permselectivity [9]. However, under such high-humidity conditions, serious

performance degradation occurs [5,10,11].

On the other hand, organic-inorganic hybrid materials have been designed and synthesized to develop novel functional materials over the last decade [12,13]. These hybrids are often synthesized through the sol-gel route using organo-substituted silicon alkoxides to afford Class II hybrids according to the classification given by Sanchez [14], where the organic and inorganic components are linked together by strong chemical bonds. In particular, the introduction of organic groups into an inorganic network can provide various tunable properties such as flexibility, solubility, hydrophobicity and negligible swelling in aqueous or organic solvents [13–15].

Polycarbosilanes (PCSs) expressed by a general formula of $[-\text{Si}(\text{CH}_3)(\text{R})-\text{CH}_2-]_n$ ($\text{R} \in \text{H}, \text{C}, \text{H}$) are well known polymer precursors for synthesizing silicon carbide (SiC)-based ceramics at $T > 1000$ °C [16,17], and they have been successfully converted to thermally stable inorganic components in the form of long fibers, filters and porous membranes [16–19].

* Corresponding author.

E-mail address: iwamoto.yuji@nitech.ac.jp (Y. Iwamoto).

However, PCSs are also appropriate as a Class II organic-inorganic hybrid: The polymer backbone composed of covalent silicon-carbon (Si-C) bond endows high flexibility, thermal and chemical stabilities of PCSs [20,21], while the methyl (CH₃) groups attached to Si atoms provide stability toward ambient moisture of PCSs, which allows PCSs to be applied as an active binder for fabricating polycrystalline SiC ceramics through the conventional powder metallurgy route [22]. More recently, PCS was found to be a useful modifier to convert hydrophilic mesoporous membrane surface into hydrophobic one [23].

The present study is firstly dedicated to the characterization of the hydrophobicity of supported PCS membranes in terms of stable gas permeations and unique preferential H₂ permeation under high humidity conditions at low-temperatures around 50 °C. By using high molecular weight PCSs having melting point above 200 °C, we showed that a superhydrophobic PCS membrane could be deposited on a mesoporous γ -Al₂O₃-modified macroporous α -Al₂O₃ tubular support. Then, gas permeation properties of the supported PCS membrane were characterized by measuring single gas permeances of helium (He), hydrogen (H₂) and nitrogen (N₂) under dry condition at 25–80 °C. Finally, the H₂-permeability was evaluated under water vapor partial pressures ranging from 0.1 to 1 at 50 °C and compared with those of a conventional sol gel-derived SiO₂ membrane. Possible mechanisms for gas permeations through the supported PCS membranes were discussed based on the gas permeation behaviors with unique H₂/He selectivity under dry condition up to 200 °C, improved H₂/N₂ selectivity under the high-humidity conditions at 50 °C and significantly high hydrophobicity of the PCSs characterized by measuring water vapor adsorption-desorption isotherms at 25 °C. Moreover, excellent H₂-selectivity under saturated humidity at 50 °C of the supported PCS membrane was demonstrated by using a H₂-N₂ (2:1) mixed feed gas as a simulated syngas produced by the novel solar hydrogen production via the PEC water-splitting reaction.

2. Experimental procedures

2.1. Synthesis of PCS membranes

In this study, commercially available PCSs (Type A, UH and UUH, Artkagaku Co., Ltd., Ibaragi, Japan) were used as received. Table 1 listed melting point (m.p.) and chemical composition of the PCSs provided by the supplier [24]. As shown in Table 1 and Fig. S1 in SEI, gel permeation chromatography (GPC) analysis at our laboratory revealed that the number average molecular weight (Mn) and the mean molecular weight (Mw) of PCS(UUH) were apparently higher than those of PCS(UH), which suggested that the m.p. of PCS(UUH) could be above 350 °C and/or no definite temperature as reported by the supplier [24].

A commercially available α -Al₂O₃ tubular support (6 mm outer diameter, 4 mm inner diameter and 60 mm length, total porosity of 40%, Noritake Co., Ltd., Aichi, Japan) was used. This α -Al₂O₃ tubular support consisted of a core with a mean pore diameter (d_{core}) of 700 nm and a rim with a d_{rim} of 150 nm.

A mesoporous γ -Al₂O₃ layer with a thickness of about 3.5 μ m was fabricated on the outer surface of the macroporous α -Al₂O₃ tubular support by following reported procedures [25,26].

Table 1
Properties of PCSs.

PCS Type	Mn/-	Mw/-	Mw/Mn	m. p./ °C [24]	Chemical composition/wt% [24]				
					Si	C	H	O	N
A	1318	4042	3.07	230	50	40	8.1	0.5	0.7
UH	1668	5920	3.55	350*	50	40	8.2	1.4	1.7
UUH	4183	8933	2.14 – n.		d.	d.	n.	n.	n.

* Partial melting.

For PCS membrane synthesis, 1 wt% solution of as-received PCS/dry xylene (super dehydrated grade, 99.5% purity, Wako Pure Chemical Co., Ltd., Osaka, Japan) was prepared for each type shown in Table 1. The PCS solution was dip-coated on the mesoporous γ -Al₂O₃ layer placed on the outer surface of the macroporous α -Al₂O₃ tubular support according to the procedures established in our previous study [23]. Then, the solvent (xylene) was removed from the PCS-coated layer by heat treatment at 120 °C to afford a PCS membrane supported on the mesoporous γ -Al₂O₃ layer placed on the outer surface of the macroporous α -Al₂O₃ tubular support (Hereafter, the supported PCS membrane was labeled as PCS(X), where X denoted type of PCS).

2.2. Characterizations

GPC measurement for as-received PCSs was performed on a Shodex GPC-104 system (Showa Denko K.K., Tokyo, Japan) equipped with two tandem columns (Shodex LF-404, Showa Denko K.K., Tokyo, Japan) calibrated against standard polystyrenes and with a Shodex RI-74S detector (Showa Denko K.K., Tokyo, Japan) using tetrahydrofuran (THF) as eluent with a flow rate of 1.0 mL min⁻¹ at 40 °C.

Water vapor adsorption-desorption isotherms of the powder samples were measured at 25 °C (Model BELSORP-aqua 3, MicrotracBEL Corp., Osaka, Japan). The powder samples of the as-received PCSs were prepared by solvent removal from the PCS(X) coating solution described above at 50 °C under vacuum followed by heat treatment at 120°C for 1 h. As a reference sample, the measurement was also performed on a SiO₂ powder prepared by drying SiO₂ sol coating solution at 60 °C for 1 h followed by heat treatment at 600 °C in air. The SiO₂ sol coating solution was prepared as follows: A mixture of 8.93 mL of tetraethoxysilane (99%, Kishida Chemical Co., Ltd., Osaka, Japan) and 8.86 mL of ethanol (99.5%, Kishida Chemical Co., Ltd., Osaka, Japan) was stirred, then peptized with a nitric acid aqueous solution of 0.357 g of HNO₃ (60.0–61.0%, Kishida Chemical Co., Ltd., Osaka, Japan) and 4.465 g of distilled water for 15 min. The peptized mixture was refluxed at 80 °C for 3 h. After cooling down to room temperature, the reaction mixture was diluted with 110.57 g of ethanol to give a SiO₂ sol coating solution for SiO₂ membrane synthesis.

Cross-sectional structure of the PCS membrane supported on the mesoporous γ -Al₂O₃ layer was observed by a scanning electron microscope (SEM, Model JSM-6360LV, JEOL Ltd., Tokyo, Japan) and examined by the energy dispersive X-ray spectroscopic (EDS) analysis (Model JSM-6010LA mounted on SEM, JEOL Ltd., Tokyo, Japan).

Single gas permeances through the supported PCS membranes were measured by the volumetric method at constant pressure. Single gas permeances under dry condition at 25–80 °C were measured in order of a kinetic diameter for He (0.26 nm), H₂ (0.289 nm) and N₂ (0.364 nm) [27]. As for the PCS(UH), the single gas permeances were measured at temperatures up to 200 °C.

Under wet condition, single gas permeances through the PCS(A) were measured at the water partial vapor pressures (p/p_0 (H₂O)) ranging from 0.1 to 1 at 50 °C. As a reference, the same measurements were performed on a sol gel-derived SiO₂ membrane fabricated as follows: The SiO₂ sol coating solution described above was dip-coated on the outer surface of the mesoporous γ -Al₂O₃-modified α -Al₂O₃ macroporous tubular support under the same manner as mentioned for the supported PCS membrane synthesis, then dried at 60 °C and subsequently heat-treated at 600 °C for 1 h. This dip coating-drying-heating process was repeated 5 times.

As for the PCS(A), gas permeances were also measured using a mixed feed gas with a 2:1 M ratio of H₂ and N₂ as a simulated syngas produced by the solar hydrogen production via the PEC water-splitting reaction.

The details of the procedures and the equipment setup for the gas permeation measurements have been reported elsewhere [23]. Single gas permeance of gas-*i* (Q_i) was calculated using Eq. (1),

$$Q_i = \frac{V_i}{S(p_1 - p_2)} \quad (1)$$

where V_i [mol s⁻¹] is the experimentally measured permeate molar flow rate of gas-*i*; S [m²] is the membrane area; p_1 [Pa] is pressure of the feed side; p_2 [Pa] is pressure of the permeate side. The pressure difference, ($p_1 - p_2$) in Eq. (1) was fixed as 100 kPa in this study.

Permselectivity was defined as the ratio of single gas permeances measured for the two kind of gases, for instance, the H₂/N₂ selectivity ($\alpha(H_2/N_2)$) was evaluated as the ratio Q_{H_2}/Q_{N_2} .

When the gas permeances were evaluated using a H₂-N₂ (2:1) mixed feed gas, the permeate gas composition was determined by using a gas chromatograph (GC, Model CP-4900 Micro-GC, Varian medical systems Inc., CA, USA) and Ar sweep gas (50 mL min⁻¹). Each gas permeance of Q_{H_2} and Q_{N_2} was evaluated by using the analyzed composition and the measured permeate molar flow rate. The water vapor permeance was evaluated using a gas chromatograph for polar gas analysis (GC323, GL Sciences Inc., Tokyo, Japan) according to the published procedure [23].

3. Results and discussion

3.1. Hydrophobicity of as-received PCSs

A significantly high hydrophobicity of as-received PCSs was characterized by measuring water vapor adsorption-desorption isotherms at 25 °C of powder samples (Fig. 1(a)). Compared with the mesoporous γ -Al₂O₃ measured in our previous study which generated a type IV-like isotherm [23], all the three types of PCSs showed a significantly low water vapor adsorption uptake and a type III isotherm, showing weak interactions between adsorbent and adsorbate. On the other hand, a reference sample, sol gel-derived SiO₂ generated a type I [28,29]-like isotherm. The slight water vapor adsorption uptake below 0.1 of $p/p_0(H_2O)$ was related to capillary condensation within the micropores [28,29]. As shown in Fig. 1(b), the maximum amount of water vapor adsorption ($V_a(H_2O)$) of the PCSs was below 4 cm³(STP)g⁻¹, which was much more lower than those of γ -Al₂O₃ (297 cm³(STP) g⁻¹) [23] and the sol gel-derived SiO₂ (39.5 cm³(STP) g⁻¹).

To examine the significantly high hydrophobic character of the PCSs in more details, FT-IR spectroscopic analysis was performed on the PCS powder samples (Fig. S2). The spectra of these samples presented common absorption peaks at 2950–2900 cm⁻¹ (ν C-H), 2100 cm⁻¹ (ν Si-H), 1450–1350 cm⁻¹ (ν C-H in CH_x (x = 1–3)), 1250 cm⁻¹ (ν

Si-CH₃), 1020 cm⁻¹ (γ CH₂ in Si-CH₂-Si) and around 800 cm⁻¹ (γ Si-CH₃ and ν Si-H in SiC₄) [17,22].

As expanded and shown in Fig. S2 in ESI, these samples exhibited a weak broad peak around 3400 cm⁻¹ attributed to intermolecular hydrogen-bonded silanol (Si-OH) group and adsorbed water molecules, while the sharp peak centered at 3674 cm⁻¹ correspond to free Si-OH group [22]. As discussed previously [23,30,31], the polar Si-OH group acted as a preferential adsorption site for water molecules. Then, density of the free Si-OH group in each sample was evaluated by measuring the relative ratio of the FT-IR absorption peak intensities: I_{Si-OH} at 3674 cm⁻¹/ I_{Si-CH_2-Si} at 1020 cm⁻¹. It was found to be as low as 0.02–0.04. Accordingly, in addition to the hydrophobic CH₃ groups attached to the Si-C backbone [22], extremely low density of the free Si-OH group lead to the superhydrophobicity of the PCSs characterized in this study.

3.2. Properties of supported PCS membranes

(1) Structure of PCS membranes

To confirm membrane formation of the PCS over the mesoporous γ -Al₂O₃ layer placed on a macroporous α -Al₂O₃ tubular support, SEM was performed through the observation of the cross-sectional SEM image of the alumina tubes functionalized by the PCS(UH) sample (Fig. 2). As a typical result, a thin dense layer with a uniform thickness of approximately 50 nm was observed on the outer surface of the mesoporous γ -Al₂O₃ layer which corresponds to the PCS(UH) membranes.

According to the EDS analysis for the cross-section (Fig. S3 in ESI), Si

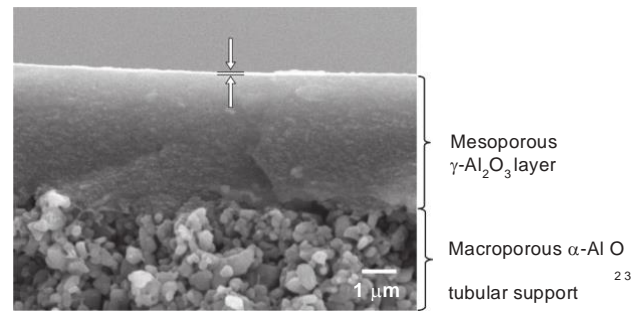


Fig. 2. A cross-sectional SEM image of PCS(UH).

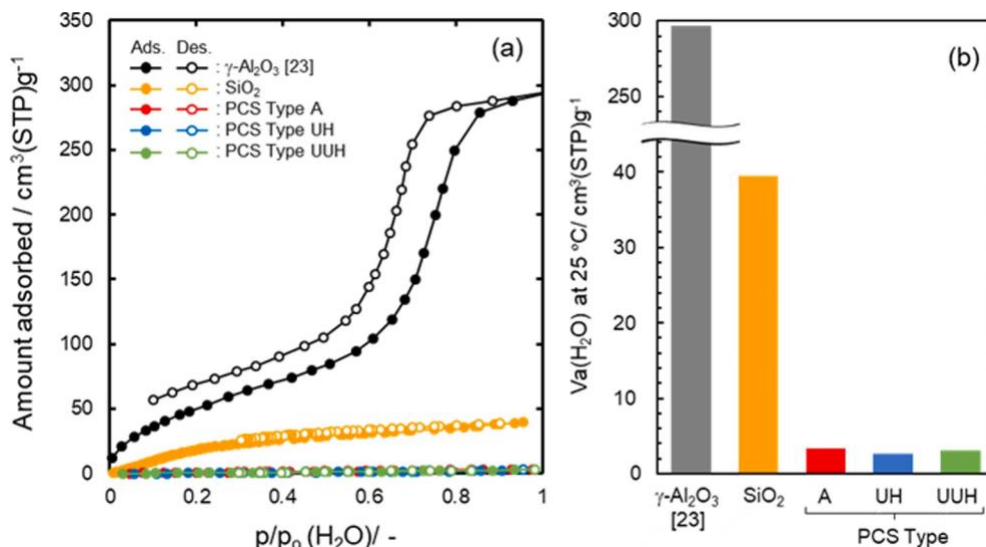


Fig. 1. Water vapor adsorption-desorption isotherms at 25 °C for (a) as-received PCSs, sol gel-derived SiO₂ and mesoporous γ -Al₂O₃ [23]. (b) Maximum amount of water vapor adsorption ($V_a(H_2O)$) at 25 °C of the PCSs in comparison with those of sol gel-derived SiO₂ and mesoporous γ -Al₂O₃ [23].

and C elements present in PCS were also detected within the mesoporous γ -Al₂O₃ layer, and it was suggested that some part of the coated PCS infiltrated the γ -Al₂O₃ mesopore channels, but located discontinuously.

(2) Gas permeation behaviors under dry condition

Fig. 3 shows Arrhenius plots of He, H₂ and N₂ permeances measured for the supported PCS membranes and Fig. 4 presents the effect of mean molecular weight (Mw) of starting PCS on the gas permeation properties at 50 °C of the supported PCS membranes shown in Fig. 3. Even at a low permeation temperature of 25 °C, the supported PCS membranes exhibited a relatively high H₂ permeance of 8.9–12 × 10⁻⁷ mol m⁻² s⁻¹ Pa⁻¹ with a H₂/N₂ permselectivity ($\alpha(H_2/N_2)$) of 11.5–13.7. Furthermore, these membranes showed a similar temperature dependence of the gas permeations: all the gas permeances linearly increased with the permeation temperature, *i.e.* following the Arrhenius law.

As we reported previously [23], gas permeations through the supported γ -Al₂O₃ layer itself was governed by the Knudsen's diffusion, and the $\alpha(H_2/N_2)$ was measured to be 3.41, which was a slight lower than the theoretical one (3.73) based on the Knudsen's diffusion. The $\alpha(H_2/N_2)$ values of the supported PCS membranes synthesized in this study were apparently higher than the theoretical one based on the Knudsen's diffusion. These superior H₂-selectivity could be provided by the PCS top-layer. However, as shown in Fig. 4, following tendencies were found: with increasing Mw of starting PCS, each gas permeance slightly increased, while $\alpha(H_2/N_2)$ decreased, *i.e.* compared with H₂, permeance of N₂ preferentially increased consistently with the Mw. These results suggested that a slight but appreciable amount of N₂ permeable pore channels by activated diffusion, *i.e.* micropore channels with a size closed to the kinetic diameter of N₂ (0.364 nm) [27] increased with Mw of the starting PCS.

The performance under dry condition of the present PCS membranes was compatible with SiO₂-based organic-inorganic hybrid membranes [32]: organic methylene (CH₂) or ethylene (CH₂CH₂) group was introduced to amorphous silica network by using 1,2-bis(triethoxysilyl) methane (BTESM) or 1,2-bis(triethoxysilyl)ethane (BTESE) as a starting silicon alkoxide for the hybrid membrane synthesis through the sol-gel route. The hybrid membranes exhibited H₂ permeance of 7.7–18 × 10⁻⁷ mol m⁻² s⁻¹ Pa⁻¹ with $\alpha(H_2/N_2)$ of approximately 12–20 at

40–50 °C [32]. However, an interesting gas permeation behavior was that, regardless of the Mw of the starting PCS, H₂ permeance was highest at all permeation temperatures from 25 to 80 °C, and the $\alpha(H_2/He)$ of the supported PCS membranes was measured to be 1.4–1.6 (Figs. 3 and 4).

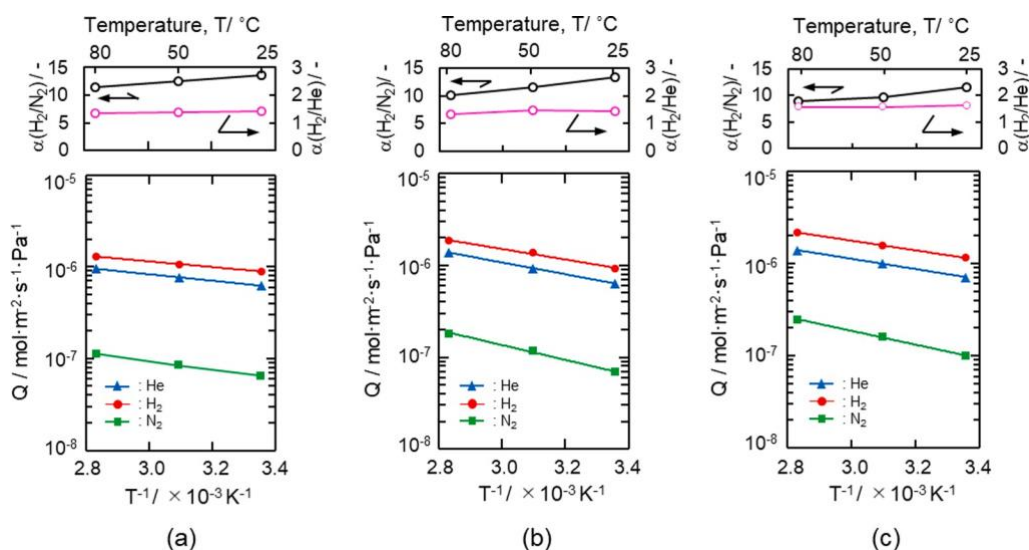


Fig. 3. Gas permeation behaviors under dry condition at 25 to 80 °C of the supported PCS membrane, (a) PCS(A), (b) PCS(UH) and (c) PCS(UUH).

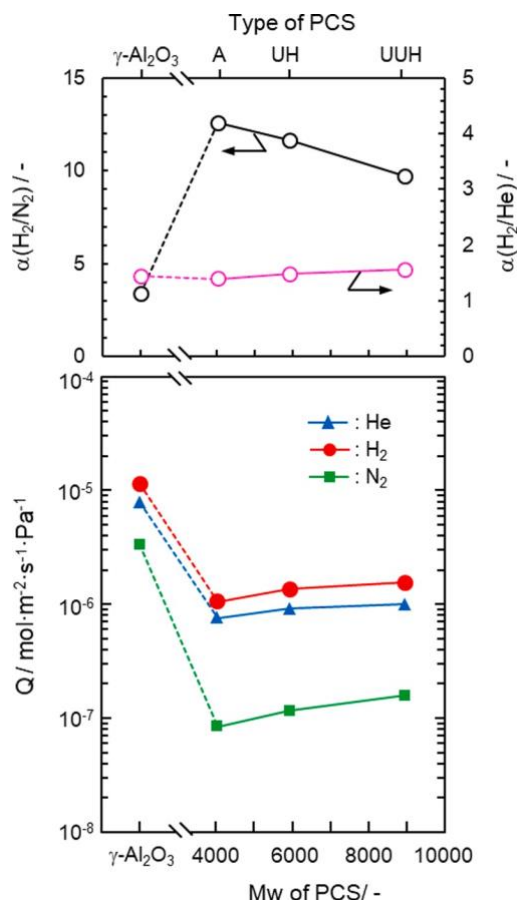


Fig. 4. Gas permeation properties at 50 °C under dry condition of PCS membranes supported on a mesoporous γ -Al₂O₃ layer as a function of Mw of starting PCS and those of the mesoporous γ -Al₂O₃ layer itself placed on a macroporous α -Al₂O₃ tubular support [23].

This result was unexpected because the permeance order of H₂ > He > N₂ did not follow the kinetic diameter of gas molecule (He: 0.26 nm, H₂: 0.289 nm and N₂: 0.364 nm) [27]. Thus, the supported PCS membranes synthesized in this study did not show simple molecular sieve properties based on the selective permeation of smaller gas molecules through micropore channels.

(3) Gas permeation behaviors under wet condition

Among the supported PCS membranes synthesized in this study, PCS (A) with the highest $\alpha(\text{H}_2/\text{N}_2)$ under dry condition was selected for further study on the gas permeation behavior under wet condition. Since the hydrogen purification process operation temperatures in the novel solar hydrogen production systems have been suggested as around 50 °C [23,33], the measurements under wet condition in this study was performed at 50 °C.

As shown in Fig. 5(a), all the gas permeances except water vapor gradually decreased with the water vapor partial pressure ($p/p_0(\text{H}_2\text{O})$). However, even under the saturated water vapor partial pressure ($p/p_0(\text{H}_2\text{O}) = 1$) at 50 °C, the PCS(A) exhibited relatively a high H_2 permeance of $7.7 \times 10^{-8} \text{ mol}^{-1} \text{ m}^{-2} \text{ s}^{-1} \text{ Pa}^{-1}$.

Under the $p/p_0(\text{H}_2\text{O})$ ranging from 0.1 to 1.0, the $\alpha(\text{H}_2/\text{He})$ was almost constant (1.1–1.3), while the $\alpha(\text{H}_2/\text{N}_2)$ increased consistently with $p/p_0(\text{H}_2\text{O})$. Especially, above $p/p_0(\text{H}_2\text{O})$ of 0.74, the $\alpha(\text{H}_2/\text{N}_2)$ rapidly increased to reach 26 at the $p/p_0(\text{H}_2\text{O}) = 1.0$. Moreover, this rapid increase was found to be associated with the drastic increase in the $\alpha(\text{H}_2\text{O}/\text{N}_2)$. At the $p/p_0(\text{H}_2\text{O}) = 1.0$, the $\alpha(\text{H}_2\text{O}/\text{N}_2)$ got to be 107 (Fig. 5(b)).

When the measurement was performed using a $\text{H}_2\text{-N}_2$ (2:1) mixed feed gas (Fig. 5(c) and (d)), the $p/p_0(\text{H}_2\text{O})$ dependency up to $p/p_0(\text{H}_2\text{O}) = 0.74$ of the membrane performance in terms of the H_2 permeance and the $\alpha(\text{H}_2/\text{N}_2)$ was quite similar to that characterized by measuring single gas permeances. However, under the $p/p_0(\text{H}_2\text{O})$ above 0.74, N_2 permeance intensively decreased. Finally, at the $p/p_0(\text{H}_2\text{O}) = 1.0$, the N_2 permeance was below the limit of detection, and the PCS(A)

was found to show an excellent H_2 -selectivity under the saturated water vapor partial pressure at 50 °C.

To investigate the gas permeation properties under the present humid conditions in more detail, the single gas permeances were measured for a reference sample, sol-gel derived SiO_2 membrane formed on the same type of mesoporous $\gamma\text{-Al}_2\text{O}_3$ -modified $\alpha\text{-Al}_2\text{O}_3$ macroporous support. As shown in Fig. 5(e), the H_2 permeance and $\alpha(\text{H}_2/\text{N}_2)$ of the supported SiO_2 membrane initially evaluated under dry condition at 50 °C were $7.1 \times 10^{-8} \text{ mol}^{-1} \text{ m}^{-2} \text{ s}^{-1} \text{ Pa}^{-1}$ and 39, respectively. Under wet condition, all the gas permeances immediately decreased at $p/p_0(\text{H}_2\text{O}) = 0.1$, then consistently decreased with $p/p_0(\text{H}_2\text{O})$. Finally, at $p/p_0(\text{H}_2\text{O}) = 1$, the He permeance was $2.1 \times 10^{-9} \text{ mol}^{-1} \text{ m}^{-2} \text{ s}^{-1} \text{ Pa}^{-1}$, while the H_2 and N_2 permeances were below the limit of detection.

It was well known that microporous SiO_2 membranes having molecular-sieving properties were beneficial to H_2 separation [9,34–38]. Actually, under the initial dry condition, the smaller kinetic diameter below 0.3 nm of the permeate gas was, the higher permeance through the present sol-gel derived SiO_2 membrane showed.

The kinetic diameter of H_2O molecule was reported as 0.265 nm [27], sufficiently smaller than the suggested mean diameter of gas-permeable micropore channels within SiO_2 (0.3 nm [9]). Water vapor could permeate through the SiO_2 membrane, which lead to the plugging of gas-permeable micropore channels by adsorption and subsequent capillary condensation of H_2O molecules as the permeate [5,10,11]; the apparent decrease in gas permeances by presence of the minute water vapor ($p/p_0(\text{H}_2\text{O}) = 0.1$) agreed well with the hydrophilic characteristics of the sol-gel derived SiO_2 shown in Fig. 1(a).

However, the rapid degradation under the higher humid condition

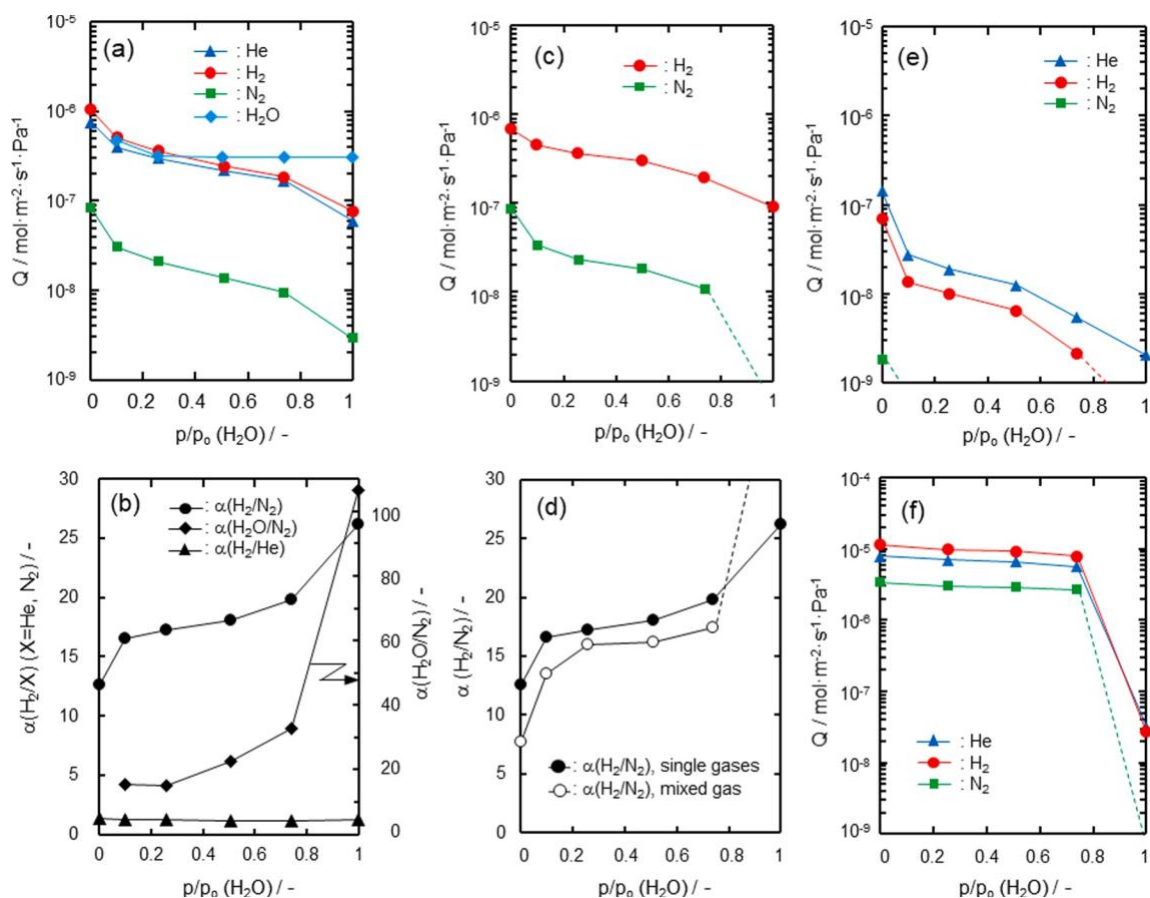


Fig. 5. Gas permeances and water vapor permeance at 50 °C evaluated for PCS(A) under $p/p_0(\text{H}_2\text{O})$ ranging from 0 to 1.0. The evaluation was performed by using (a), (b) single gases of He, H_2 and N_2 and (c) a mixed gas of H_2 and N_2 in the molar ratio 2:1. (d) Comparison of $\alpha(\text{H}_2/\text{N}_2)$ values evaluated based on the single gas permeances and those by using the $\text{H}_2\text{-N}_2$ (2:1) mixed feed gas. Gas permeances evaluated for reference samples, (e) supported SiO_2 membrane and (f) supported mesoporous $\gamma\text{-Al}_2\text{O}_3$ membrane itself [23] under $p/p_0(\text{H}_2\text{O})$ ranging from 0 to 1.0 at 50 °C.

above p/p_0 (H_2O) of 0.5 was inconsistent with the H_2O adsorption behavior shown in Fig. 1(a): At around p/p_0 (H_2O) = 0.4, the amount of water vapor adsorption measured for the SiO_2 reached maximum, while both He and H_2 permeances decreased rather rapidly above p/p_0 (H_2O) = 0.5 (Fig. 5(e)). This was due to the high hydrophilicity of the mesoporous $\gamma-Al_2O_3$ layer beneath the SiO_2 membrane. As we reported in our previous study [23], above p/p_0 (H_2O) 0.4, the water vapor adsorption-desorption isotherm for the sol-gel derived mesoporous $\gamma-Al_2O_3$ exhibited a large hysteresis loop assigned to capillary condensation of H_2O molecules within mesopores, which lead to the drastic decrease in gas permeances through the supported mesoporous $\gamma-Al_2O_3$ layer itself under the high-humidity conditions at 50 °C (Fig. 5(f) [23]). Accordingly, in addition to the intrinsic degradation by the permeate H_2O -induced plugging within the SiO_2 membrane, gas permeations through the supported SiO_2 membrane could be intensively restricted by condensation of the permeate H_2O molecules within mesopores located close to the hetero interface between the $\gamma-Al_2O_3$ layer and the top surface SiO_2 membrane.

As shown in Fig. 5(a), the PCS(A) exhibited a relatively high water vapor permeance of $3.1 \times 10^{-7} \text{ mol}^{-1} \text{ m}^{-2} \text{ s}^{-1} \text{ Pa}^{-1}$ at the p/p_0 (H_2O) = 1.0. This value was compatible with that previously measured for the supported mesoporous $\gamma-Al_2O_3$ layer itself ($7.1 \times 10^{-7} \text{ mol}^{-1} \text{ m}^{-2} \text{ s}^{-1} \text{ Pa}^{-1}$) [23]. Thus, gas permeation property of the PCS(A) could be also affected by the highly hydrophilic character of the mesoporous $\gamma-Al_2O_3$ layer. However, an interesting point was that the affection in terms of the decrease in permeance under the high-humidity conditions was mainly observed for N_2 gas, and such affection was more pronounced when the gas permeation measurement was performed by using a mixed H_2-N_2 (2:1) gas (Fig. 5(c)). These results suggested that the dominant permeation of N_2 and water vapor was diffusion through micropore channels within the PCS top-layer network. Under higher humid conditions above p/p_0 (H_2O) = 0.74, N_2 permeation was thought to be restricted by the highly hydrophilic mesoporous $\gamma-Al_2O_3$ layer as in the case of the supported SiO_2 membrane discussed above. On the other hand, the He and H_2 permeations through the PCS(A) were thought to be governed by diffusion through the hydrophobic and dense PCS top-layer network where neither H_2O nor N_2 could permeate.

3.3. Analysis of gas permeation behaviors

(1) He and H_2 permeations

In order to quantitatively explain the mechanism of He and H_2 permeation through the PCS top-layer network, the He and H_2 permeances were measured at room temperature to 200 °C (sufficiently high above 150 °C to examine the affection by physisorption of gas molecules [37,38]), and analyzed using a solid-state diffusion model [39–42]. In this analysis, another membrane sample, PCS(UH) having a higher m.p. (350 °C) was adopted.

Solid-state diffusion occurs with further decrease in the pore size than Knudsen diffusion occurs, where the gas molecule interacts strongly with the membrane material behaving as a dense material. In this case, the solubility of the gas molecule is necessary to consider, so that the molecules permeance through the membrane (Q) can be expressed by the product of the solubility and the diffusivity. The solubility (S) is derived from the equilibrium between the solubility sites and the gaseous phase [43]. The diffusivity (D) is supposed that the process of gas atom movement between solubility sites in the membrane is a random walk process with an equilibrium established between atoms in solubility sites and those moving between sites [44]. Gas molecules, vibrating at solubility sites with a characteristic frequency, jump to an adjacent solubility site by surmounting a potential barrier. The permeance ($Q=SD$) is given by following equation, considering the effect of rotation of polyatomic gas molecule:

$$Q_{ss} = \frac{d^2 h^2}{6L} \left(\frac{1}{2\pi m k T} \right)^{\frac{1}{2}} \left(\frac{\sigma h^2}{8\pi^2 I k T} \right)^{\alpha} \times \frac{(N_s/N_A)}{e^{h\nu^* 2kT} e^{-h\nu^* 2kT} 2e^{-\frac{\Delta E_{ss}}{RT}}} \quad (2)$$

where Q_{ss} is the permeance through the membrane [$\text{mol m}^{-2} \text{ s}^{-1} \text{ Pa}^{-1}$], d is jump distance [m], h is Planck's constant [$\text{m}^2 \text{ kg s}^{-1}$], L is the thickness of the membrane [m], m is the mass [kg], ν^* is vibrational frequency of the gas molecules in the passageways between the sorption sites [s^{-1}], k is Boltzmann's constant [J K^{-1}], T is the temperature [K], σ is the symmetry factor of the species ($\alpha=2$ for H_2), I is the moment of inertia [kg m^2], N_s is number of solubility sites per area [m^{-3}], N_A is Avogadro's number [mol^{-1}], ΔE_{ss} is activation energy for permeation [J mol^{-1}], α is an exponent accounting for incomplete loss of rotation ($\alpha = 0$ for monoatomic molecule, He, and $\alpha=0.2$ for polyatomic molecule, H_2), R is the gas constant [$\text{J mol}^{-1} \text{ K}^{-1}$].

As shown in Fig. 6(a), at all temperatures up to 200 °C (473 K), the experimental permeance of H_2 was higher than that of He, and each gas permeance monotonously increased with the permeation temperature. Then, the temperature dependence of the He and H_2 permeances were fitted to the non-linear curve by the Eq. (2) with three free parameters, N_s , ν^* and ΔE_{ss} which were determined using Igor Pro 7.00 (wave-metrics, Inc., OR, USA). The membrane thickness (L) was 50 nm as obtained from the SEM image shown in Fig. 2 and jump distance (d) was 0.8 nm which was used by following previous reports [39,45]. The calculated permeances of He and H_2 were well consistent with experimental data, so that the solid-state diffusion model fitting analysis was to be made appropriately.

The fitting parameters obtained in this study were listed in Table 2, and compared with those for H_2 -selective amorphous ceramic membranes previously reported by other research groups: polysiloxane-derived amorphous silicon oxycarbide (SiOC) membrane (#01) synthesized by pyrolysis at 700 °C in Ar [45], and CVD-derived SiO_2 membranes (#02 ~ 05) having different microporosity which Oyama et al. [41,42,46,47] systematically synthesized by varying the organic ligand of starting Si alkoxide precursor and CVD process temperature in Ar: #02 [46] and #03 [41] (tetraethoxysilane (TEOS) at 600 °C), #04 (vinyltriethoxysilane (VTES) at 600 °C) [42], #05 (35% trimethylmethoxysilane (TMMOS) -TEOS at 650 °C) [47].

There were two criteria for this curve fitting study: (1) N_s , the number of solubility sites should be in inverse relation to the kinetic diameter of the permeate gas molecule because the larger gas molecule could not fit into more solubility sites, and thus N_s for H_2 (0.289 nm) < N_s for He (0.26 nm). (2) ν^* , the vibrational frequency should be higher for the permeate gas having the smaller molecular weight, i.e., ν^* for H_2 (2.02 g mol^{-1}) > ν^* for He (4.00 g mol^{-1}). As shown in Table 2, the values of N_s and ν^* estimated for He and H_2 permeations through the PCS(UH) corresponded to the physical constants mentioned above, and similar to those previously reported for the membranes composed of SiOC (#01) [45] or SiO_2 (#02 ~ 05) [41,42,46,47].

Due to several differences in material factors of the network which composing active separation layer such as chemical composition and density, it was difficult to discuss on the difference in the fitting parameters, however, the values of N_s for He and H_2 permeations through the present PCS top-layer were compatible with those reported for the CVD-derived SiO_2 membrane (#05) with relatively low density, fabricated by using starting Si alkoxides having organic ligands such as 35% TMMOS-TEOS [47]. On the other hand, the ν^* values for both He and H_2 were apparently lower than those reported for the CVD-derived SiO_2 membranes (#02 ~ 05) [41,42,46,47], but were approximately one order of magnitude higher than those reported for the polymer-derived SiOC membrane (#01) [45].

One unique result was the ΔE_{ss} , activation energy obtained for the present PCS top-layer. ΔE_{ss} has an inverse relationship with N_s physically, because the larger molecules must overcome a larger energy barrier to migrate through the membrane. In this context, all the data reported for the SiO_2 membranes (#02 ~ 05) followed this relation, and

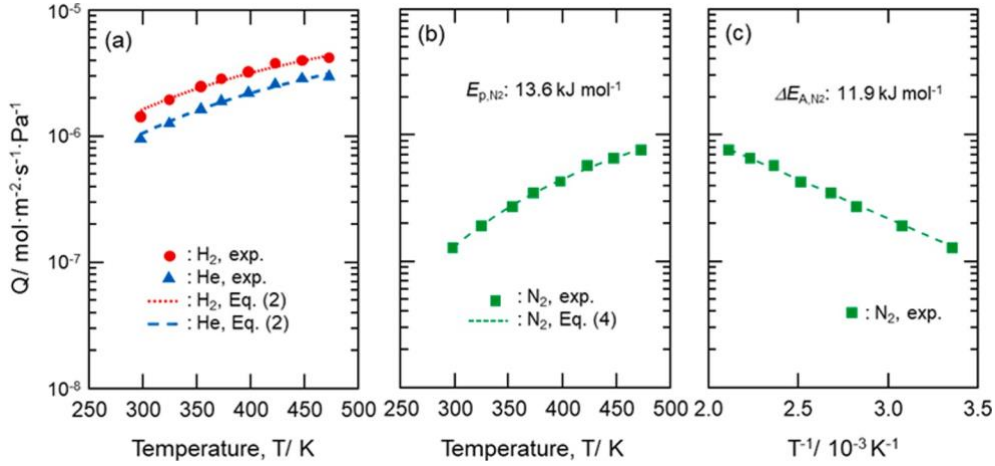


Fig. 6. Study on temperature dependence of gas permeances through the PCS(UH) at room temperature to 473 K (200 °C). Comparison of experimentally evaluated (a) H₂ and He permeances with those calculated using solid-state diffusion model (Eq. (2)) and (b) N₂ permeances with those calculated based on the modified gas-translational diffusion model (Eq. (4)). (c) Arrhenius plot of the experimentally evaluated N₂ permeances.

Table 2
Comparison of H₂ permeation properties and fitting parameters.

No.	Membrane	H ₂ permeation properties				$N_2/10^{25} \text{ m}^{-3}$		$v^*/10^{12} \text{ s}^{-1}$		$\Delta E_{ss}/\text{kJ mol}^{-1}$		
		T/K	Q/H	$Q_2/\text{mol m}^{-2} \text{ s}^{-1} \text{ Pa}^{-1}$	$\alpha(\text{H}_2/\text{X})/^\circ$	X	He	H ₂	He	H ₂	He	H ₂
This work	PCS(UH)	323		1.4×10^{-6}	11.7	N ₂	15.0	11.0	0.60	0.66	5.9	5.8
#01	SiOC [45]	573		1.78×10^{-8}	22.4	N ₂	1.3	0.76	0.082	0.089	8.5	7.9
#02	SiO ₂ [46]	873		1.2×10^{-7}	1800	CO	74.0	27.3	7.77	8.10	8.0	12.8
#03	SiO ₂ [41]	873		5.0×10^{-7}	5100	CO	62	38	7.0	7.3	4.2	10.4
#04	SiO ₂ [42]	873		5.4×10^{-7}	150	N ₂	47.5	33.5	2.21	2.39	3.4	7.3
#05	SiO ₂ [47]	923		1.1×10^{-6}	53	N ₂	15.7	8.7	2.94	3.02-0.08	1.86	

the ΔE_{ss} for H₂ permeation was apparently higher than that of He [41,42,46,47]. On the other hand, the ΔE_{ss} for H₂ permeation through the PCS top-layer was evaluated as 5.8 kJ mol⁻¹ and found to be rather slight lower than that for the He permeation (5.9 kJ mol⁻¹). This result corresponded well with the unique H₂-permselectivity experimentally observed for the PCS(UH), H₂ permeance increased consistently with temperature, and at all temperatures up to 200 °C, the permeance of H₂ was higher than that of the smaller gas molecule of He (Fig. 6(a)).

Gurol *et al.* reported that the polymer-derived SiOC membrane (#01) exhibited a similar H₂-permselectivity, and as shown in Table 2, their fitting study also resulted in the irregular relation, $\Delta E_{ss}/\text{kJ mol}^{-1}$ for He permeation (8.5) > for H₂ permeation (7.9) [45]. The PCS top-layer investigated in this study was ternary SiCH organic-inorganic hybrid polymer composed Si-C backbone substituted with considerable amount of CH₃ groups. Accordingly, it was suggested that the existence of such hydrocarbon groups allowed preferential dissolution and subsequent diffusion of H₂ explained by the solid-state diffusion mechanism discussed above. Moreover, it was found that the ΔE_{ss} (5.8 kJ mol⁻¹) for the H₂ permeation through the present PCS membrane was much lower than

those (16.3–16.7 kJ mol⁻¹) of silicon oxycarbide (SiOC) membranes derived from polydimethylsilane (PMS) reported by Tsai *et al.* [48]. According to the reported membrane syntheses route, prior to the final pyrolysis at 300–600 °C, PMS was thermally converted to PCS via the Kumada rearrangement during the heat treatment at 460 °C for 14 h under Ar, then cured at 200 °C in air for 1 h. The PCS formed in-situ could be highly reactive to be well cross-linked during the long-time heat treatment at 460 °C. Moreover, the heat-treated PCS became infusible via Si–O–Si bond formations by the subsequent curing in air. These thermal treatments led to the formation of dense network like microporous amorphous SiO₂ in spite of the final low-temperature pyrolysis at 300 to 600 °C.

(2) N₂ permeation

In addition to He and H₂ permeances, the temperature dependence of N₂ permeance was measured for the same PCS(UH). As shown in Fig. 6 (b), N₂ permeance also increased consistently with permeation temperature.

As discussed above, the dominant permeation of N₂ could be diffusion through micropore channels within the PCS top-layer network. Then, the temperature dependence of the N₂ permeance was examined using a permeation model equation recently proposed by Yoshioka *et al.* [37], which considering the effect of the potential field in a micropore [37,49]:

$$Q = \frac{k_0}{\sqrt{RT}} \left(d - d_i \right) \exp \left(- \frac{E_{act,i} + E_{att,i}}{RT} \right), k_0 = \frac{N_p \sqrt{F}}{6\tau A_m L} \quad (3)$$

where Q_{ckl} [mol m⁻² s⁻¹ Pa⁻¹] is the Knudsen permeance of gas molecules that are concentrated by the attractive nature of the potential field of pore wall, d_0 is native pore diameter [m], d_i is kinetic diameter of

i -th component [m], N_p is the number of pores with pore diameters of d_0 on the membrane, τ is the tortuosity [-], A_m is the membrane area [m²], L is the thickness of the membrane [m], M_i is the molar weight of the i -th diffusing gas component [kg mol⁻¹], $E_{act,i}$ is the activation energy for the permeation of the i -th component [J mol⁻¹], $E_{att,i}$ is the attractive potential energy for the i -th component [J mol⁻¹], R is the gas constant [J mol⁻¹ K⁻¹], and T is the permeation temperature [K].

Eq. (3) is a modified gas-translational (GT) diffusion [50–52] (mGT) model equation with the additional consideration of the effective diffusion length ($d_0 - d_i$) and provides a more detailed description of the gas permeation model equation by considering activation energy, adsorption energy and size of permeate gas molecule. Accordingly, the mGT model can be expected to achieve universal understandings of the permeation mechanisms in a micropore from Knudsen diffusion to

activated diffusion [37,49].

In this study, $Q_{e,kl}$ was renamed as Q_{mGT} and expressed by simplifying Eq. (3) as:

$$Q_{mGT} = \frac{k_0}{M_i} \exp\left(-\frac{E_{p,i}}{RT}\right) \quad (4)$$

where $k_{0,i} = k_0 (d_0 - d_i)^3$, and $E_{p,i} = E_{act,i} + E_{att,i}$. Then, the value of $E_{p,i}$ for the N_2 permeation was estimated by fitting Eq. (4) to the experimentally obtained temperature dependency data with two free parameters, $k_{0,i}$ and $E_{p,i}$. These parameters were also determined using Igor Pro 7.00. As shown in Fig. 6(b), the calculated permeance of N_2 was well consistent with experimental data, and the fitting parameter, $E_{p,i}$ was found as 13.6 kJ mol⁻¹.

As we reported previously, the PCSs exhibited extremely low affinity toward N_2 , and it was impossible to measure the BET (Brunauer-Emmett-Teller) surface area by using N_2 as a probe molecule at 77 K [31]. Accordingly, even at room temperature, the E_{att,N_2} could be negligibly small, and thus $E_{p,N_2} \approx E_{act,N_2}$. Moreover, the E_{p,N_2} was compatible with the activation energy for N_2 permeation ($\Delta E_{A,N_2}$, 11.9 kJ mol⁻¹) obtained by the Arrhenius plot (Fig. 6(c)). The dominant mechanism for the N_2 permeation could be recognized as activated diffusion, which indicated that the PCS top-layer had a microporosity with the size of pore channels close to the kinetic diameter of N_2 gas

molecule (0.364 nm).

(3) Effect of water vapor partial pressure on gas permeations

A schematic diagram of Fig. 7 presents possible gas permeation behaviors through the PCS membrane supported on a mesoporous γ - Al_2O_3 layer investigated in this study.

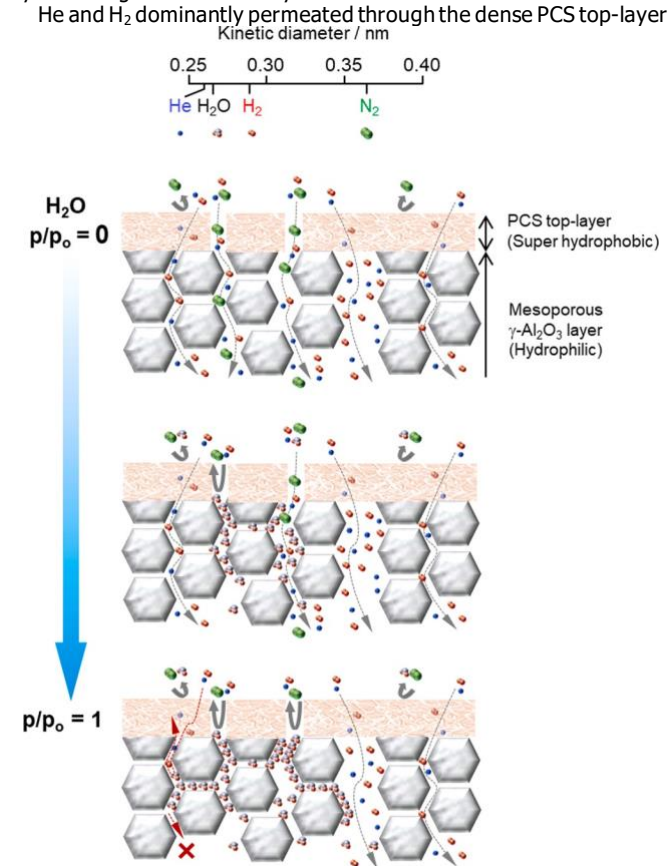


Fig. 7. Schematic of gas permeation behaviors through a PCS membrane supported on a mesoporous γ - Al_2O_3 layer under dry and wet conditions at 50 °C.

network governed by the solid-state diffusion mechanism, while the dominant N_2 permeation was activated diffusion through the micropore channels within the PCS network. The size of the micropore channels could be close to the kinetic diameter of N_2 (d_{N_2} , 0.364 nm) [27].

The kinetic diameter of water vapor (H_2O molecule, 0.265 nm) [27] was sufficiently smaller than d_{N_2} . Moreover, the PCS was highly hydrophobic, which allowed stable water vapor permeation through the N_2 -permeable micropore channels within the PCS top-layer. However, immediate adsorption and subsequent condensation of the permeate H_2O molecules could proceed at the entrance to the highly hydrophilic mesoporous γ - Al_2O_3 layer beneath the PCS top-layer, i.e. at the hetero interface between the PCS layer and mesoporous γ - Al_2O_3 layer.

Then, the relationship between the $p/p_0(H_2O)$ and degree of the permeate H_2O -induced plugging was examined in the following attempt: The entrance to the mesoporous γ - Al_2O_3 layer was treated as a cylindrical pore having a mean effective diameter, d_{ent} . Under the $p/p_0(H_2O)$ ranging from 0.1 to 1.0, the d_{ent} was estimated by calculating the normalized Knudsen-based permeance (NKP) f_{NKP} , which is defined as the ratio of the permeance of a target component (Q_i) to standard gas permeance (Q_s), that considers the contribution of molar weight can be given as a function of gas molecular size, d_i by measuring the gas permeances of several gases at a given constant temperature [37],

$$f_{NKP} = \frac{Q_i}{Q_s} = \frac{M_i}{M_s} \left(\frac{d_{ent} - d_s}{d_i - d_s} \right)^3 \exp\left(-\frac{E_{p,i}}{RT}\right) \approx \left(\frac{d_{ent}}{d_i} \right)^3 \quad (5)$$

Under the limiting conditions of $d_s < d_i < d_{ent}$, kinetic diameter depending on the f_{NKP} was fitted to the non-linear curve by Eq. (5) with two free parameters: f_{NKP} and d_{ent} , which were determined using Igor Pro 7.00. The values of f_{NKP} were calculated using the permeance through the PCS(A) under dry and wet condition at 323 K (50 °C) shown in Fig. 5(a). The permeance and molecular size of He were adopted as Q_s and d_s , respectively. In this estimation, the plots for H_2O and H_2 were excluded from the fitting, because H_2O was condensable under the present wet condition, while H_2 preferentially permeated through the PCS top-layer. The results are shown in Fig. S4 in ESI. For comparison, the f_{NKP} values for H_2O and H_2 were marked or listed in this graph. The d_{ent} under the initial dry condition was estimated as 0.57 nm, then got to be smaller consistently with the $p/p_0(H_2O)$. Finally, the d_{ent} at $p/p_0(H_2O) \approx 0$ was estimated as 0.47 nm.

The d_{ent} values estimated were indeed large enough for all the gases of He, H_2 and N_2 to permeate through, but plugging of a certain fraction of the entrance having a much smaller diameter (closed to d_{N_2} , 0.364 nm) could proceed under the high-humidity conditions of $p/p_0(H_2O) > 0.5$ at 50 °C.

As shown in Fig. 5(a), there was a tendency that all the gas permeances decreased with increasing $p/p_0(H_2O)$, which could be due to the increase in the pressure drop caused by increasing amount of the H_2O molecules condensed at around the hetero interface. This affection was more pronounced in the case using the H_2 - N_2 (2:1) mixed feed gas, i.e. when the driving force for N_2 gas permeation was reduced by decreasing the partial pressure difference between the gas feed side and permeate side of the membrane under the saturated water vapor partial pressure at 50 °C (Fig. 5(c) and (d)). On the other hand, at $p/p_0(H_2O) > 0.1$, the water vapor exhibited a stable permeation with a relatively high permeance of approximately 3.0×10^{-7} [mol m⁻² s⁻¹ Pa⁻¹] at 50 °C (Fig. 5(a)). The observed water vapor permeation was thought to be governed by the surface diffusion/capillary condensation along with the extremely hydrophilic γ - Al_2O_3 mesopore wall.

4. Summary

In the present study, super hydrophobicity of PCSs was characterized by measuring water vapor adsorption-desorption isotherms at 25 °C.

Then, the PCS membrane with a thickness of about 50 nm was successfully formed over a mesoporous γ -Al₂O₃ layer placed on an outer surface of a macroporous α -Al₂O₃ tubular support. Under dry and wet condition, gas permeances through the supported PCS membranes were assessed and discussed to clarify their possible permeation mechanisms. The results can be summarized as follows:

- (1) Water vapor adsorption-desorption isotherms measurements revealed that the amount of water adsorption under the saturated water vapor partial pressure at 25 °C of the PCSs was below 4 cm³(STP) g⁻¹, which showed significantly high hydrophobicity.
- (2) Under dry condition at 50 °C, the supported membrane synthesized using PCS having Mw of 4042 (PCS(A)) exhibited the best membrane performance: the H₂ permeance of 1.4×10^{-6} mol⁻¹ m⁻² s⁻¹ Pa⁻¹ and α (H₂/N₂) of 12.6 together with unique α (H₂/He) of 1.4.
- (3) Even under saturated water vapor partial pressure at 50 °C, the PCS(A) kept a relatively high H₂ permeance of 7.7×10^{-8} mol⁻¹ m⁻² s⁻¹ Pa⁻¹ with improved H₂/N₂ selectivity of 26.
- (4) The dominant mechanism for He and H₂ permeations through the PCS top-layer was suggested as solid state diffusion. The activation energy for the H₂ permeation was estimated as 5.8 kJ mol⁻¹ and was found to be slightly lower than that for the He permeation (5.9 kJ mol⁻¹).
- (5) The activation energy for N₂ permeation through the supported PCS membrane was estimated by using the mGT model as 13.6 kJ mol⁻¹. This value was compatible with that obtained by the conventional Arrhenius plot (11.9 kJ mol⁻¹).
- (6) The enhanced H₂-permselectivity observed under the high-humidity conditions at 50 °C was explained by the synergistic effect of the preferential H₂ permeation through the dense PCS top-layer network and blockage of N₂ permeation pathway by the permeate H₂O-induced plugging. As a result, when the H₂-N₂ (2:1) mixed feed gas was used for measuring gas permeances under saturated humidity at 50 °C, the N₂ permeance was below the limit of detection, which showed great potential of PCSs to develop high-performance membranes for hydrogen recovery from the syngas produced by the novel solar hydrogen production systems.

Funding

This work was in part supported by "Research Project for Future Development: Artificial Photosynthetic Chemical Process (ARPChem)" (METI/NEDO, Japan: 2012-2022). Dr. Samuel Bernard and Prof. Yuji Iwamoto would like to thank CNRS who financially supported present work via the International Research Project (IRP) 'Ceramics materials for societal challenges'.

References

- [1] K. Maeda, K. Domen, New non-oxide photocatalysts designed for overall water splitting under visible light, *J. Phys. Chem. C* 111 (2007) 7851–7861, <https://doi.org/10.1021/jp070911w>.
- [2] Q. Wang, T. Hisatomi, Q. Jia, H. Tokudome, M. Zhong, C. Wang, Z. Pan, T. Takata, M. Nakabayashi, N. Shibata, Y. Li, I.D. Sharp, A. Kudo, T. Yamada, K. Domen, Scalable water splitting on particulate photocatalyst sheets with a solar-to-hydrogen energy conversion efficiency exceeding 1%, *Nat. Mater.* 15 (2016) 611–615, <https://doi.org/10.1038/nmat4589>.
- [3] Y. Goto, T. Hisatomi, Q. Wang, T. Higashi, K. Ishikiriyama, T. Maeda, Y. Sakata, S. Okunaka, H. Tokudome, M. Katayama, S. Akiyama, H. Nishiyama, Y. Inoue, T. Takewaki, T. Setoyama, T. Minegishi, T. Takata, T. Yamada, K. Domen, A particulate photocatalyst water-splitting panel for large-scale solar hydrogen generation, *Joule* 2 (2018) 509–520, <https://doi.org/10.1016/j.joule.2017.12.009>.
- [4] S. Yagyu, H. Matsui, T. Matsuda, H. Yasumoto, Studies of explosive characteristics of hydrogen (1st report), *Minist. Labour, Res. Inst. Ind. Saf.* (1969).
- [5] K. Tanaka, Y. Sakata, Present and future prospects of hydrogen production process constructed by the combination of photocatalytic H₂O splitting and membrane separation process, *Membrane* 36 (2011) 113–121, <https://doi.org/10.5360/membrane.36.113>.
- [6] H. Yin, A.C.K. Yip, A review on the production and purification of biomass-derived hydrogen using emerging membrane technologies, *Catalysts* 7 (2017) 297, <https://doi.org/10.3390/catal7100297>.
- [7] S.T. Oyama, S.M. Stagg-Williams, *Inorganic, Polymeric and Composite Membranes: Structure, Function and Other Correlations*, Elsevier, Amsterdam, 2011.
- [8] T. Yamaguchi, A. Takagaki, T. Sugawara, R. Kikuchi, S.T. Oyama, Supported fluorocarbon liquid membranes for hydrogen/oxygen separation, *J. Memb. Sci.* 520 (2016) 272–280, <https://doi.org/10.1016/j.memsci.2016.07.010>.
- [9] Y. Iwamoto, Precursors-derived ceramic membranes for high-temperature separation of hydrogen, *J. Ceram. Soc. Jpn* 115 (2007) 947–954, <https://doi.org/10.2109/jcersj2.115.947>.
- [10] A. Burneau, J. Lepage, G. Maurice, Porous silica-water interactions. I. Structural and dimensional changes induced by water adsorption, *J. Non. Cryst. Solids* 217 (1997) 1–10, [https://doi.org/10.1016/S0022-3093\(97\)00113-0](https://doi.org/10.1016/S0022-3093(97)00113-0).
- [11] T. Tsuru, T. Hino, T. Yoshioka, M. Asaeda, Permporometry characterization of microporous ceramic membranes, *J. Memb. Sci.* 186 (2001) 257–265, [https://doi.org/10.1016/S0376-7388\(00\)00692-X](https://doi.org/10.1016/S0376-7388(00)00692-X).
- [12] J. Wen, G.L. Wilkes, Organic/inorganic hybrid network materials by the sol-gel approach, *Chem. Mater.* 8 (1996) 1667–1681, <https://doi.org/10.1021/cm9601143>.
- [13] U. Díaz, A. Corma, Organic-inorganic hybrid materials: multi-functional solids for multi-step reaction processes, *Chem. - A Eur. J.* 24 (2018) 3944–3958, <https://doi.org/10.1002/chem.201704185>.
- [14] P. Judeinstein, C. Sanchez, Hybrid organic-inorganic materials: a land of multidisciplinary, *J. Mater. Chem.* 6 (1996) 511–525, <https://doi.org/10.1039/JM9960600511>.
- [15] C. Sanchez, B. Julián, P. Belleville, M. Popall, Applications of hybrid organic-inorganic nanocomposites, *J. Mater. Chem.* 15 (2005) 3559–3592, <https://doi.org/10.1039/b509097k>.
- [16] S. Yajima, J. Hayashi, M. Omori, Continuous silicon carbide fiber of high tensile strength, *Chem. Lett.* 4 (1975) 931–934, <https://doi.org/10.1246/cl.1975.931>.
- [17] S. Yajima, K. Okamura, J. Hayashi, M. Omori, Synthesis of continuous SiC fibers with high tensile strength, *J. Am. Ceram. Soc.* 59 (1976) 324–327, <https://doi.org/10.1111/j.1151-2916.1976.tb10975.x>.
- [18] F. Sandra, A. Ballester, V.L. Nguyen, M.N. Tsampas, P. Vernoux, C. Balan, Y. Iwamoto, U.B. Demirci, P. Miele, S. Bernard, Silicon carbide-based membranes with high soot particle filtration efficiency, durability and catalytic activity for CO/HC oxidation and soot combustion, *J. Memb. Sci.* 501 (2016) 79–92, <https://doi.org/10.1016/j.memsci.2015.12.015>.
- [19] D. Hotza, M. Di Luccio, M. Wilhelm, Y. Iwamoto, S. Bernard, J.C. Diniz da Costa, Silicon carbide filters and porous membranes: a review of processing, properties, performance and application, *J. Memb. Sci.* 610 (2020), 118193, <https://doi.org/10.1016/j.memsci.2020.118193>.
- [20] L.V. Interrante, Q. Shen, Polycarbosilanes, in: R.G. Jones, W. Ando, J. Chojnowski (Eds.), *Silicon-Containing Polym.*, Kluwer Academic Publisher, Netherlands, 2000, pp. 247–321. ISBN: 9780412831102.
- [21] K. Matsumoto, Polycarbosilanes, in: H.F. Mark (Ed.), *Encycl. Polym. Sci. Technol.*, John Wiley & Sons, New York, 2003, pp. 426–438. ISBN: 978-1-118-63389-2.
- [22] Y. Sawai, Y. Iwamoto, S. Okuzaki, Y. Yasutomi, K. Kikuta, S. Hirano, Synthesis of silicon carbide ceramics using chemically modified polycarbosilanes as a compaction binder, *J. Am. Ceram. Soc.* 82 (1999) 2121–2125, <https://doi.org/10.1111/j.1151-2916.1999.tb02051.x>.
- [23] M. Kubo, M. Kojima, R. Mano, Y. Daiko, S. Honda, Y. Iwamoto, A hydrostable mesoporous γ -Al₂O₃ membrane modified with Si–C–H organic-inorganic hybrid derived from polycarbosilane, *J. Memb. Sci.* 598 (2020), 117799, <https://doi.org/10.1016/j.memsci.2019.117799>.
- [24] Currently, polycarbosilanes ("Nipusi®") are available from Artkagaku Co. Ltd., <http://www.artkagaku.co.jp/contact/index.html>.

- [25] M.H. Zahir, K. Sato, Y. Iwamoto, Development of hydrothermally stable sol-gel derived La_2O_3 -doped Ga_2O_3 - Al_2O_3 composite mesoporous membrane, *J. Memb. Sci.* 247 (2005) 95–101, <https://doi.org/10.1016/j.memsci.2004.09.011>.
- [26] M.H. Zahir, K. Sato, H. Mori, Y. Iwamoto, M. Nomura, S.I. Nakao, Preparation and properties of hydrothermally stable γ -alumina-based composite mesoporous membranes, *J. Am. Ceram. Soc.* 89 (2006) 2874–2880, <https://doi.org/10.1111/j.1551-2916.2006.01165.x>.
- [27] D.W. Breck, *Zeolite Molecular Sieves: Structure, Chemistry, and Use*, John Wiley & Sons, New York, 1974 <https://doi.org/10.1093/chromsci/13.4.18A-c>.
- [28] K.S.W. Sing, D.H. Everett, R.A.W. Haul, L. Moscou, R.A. Pierotti, J. Rouquerol, T. Siemienieska, Reporting physisorption data for gas/solid systems with special reference to the determination of surface area and porosity, *Pure Appl. Chem.* 57 (1985) 603–619. ISBN: 978-1-4020-2303-3.
- [29] S. Lowell, J.E. Shields, M.A. Thomas, M. Thommes, *Characterization of Porous Solids and Powders*, Springer, Netherlands, 2004.
- [30] M.N. Mohd Sokri, T. Onishi, Y. Daiko, S. Honda, Y. Iwamoto, Hydrophobicity of amorphous silica-based inorganic-organic hybrid materials derived from perhydropolysilazane chemically modified with alcohols, *Microporous Mesoporous Mater.* 215 (2015) 183–190, <https://doi.org/10.1016/j.micromeso.2015.05.039>.
- [31] Z. Mouline, K. Asai, Y. Daiko, S. Honda, S. Bernard, Y. Iwamoto, Amine-functionalized polycarbosilane hybrids for CO_2 -selective membranes, *J. Eur. Ceram. Soc.* 37 (2017) 5213–5221, <https://doi.org/10.1016/j.jeurceramsoc.2017.04.008>.
- [32] X. Ren, T. Tsuru, Organosilica-based membranes in gas and liquid-phase separation, *Membranes* 9 (2019) 107, <https://doi.org/10.3390/membranes9090107>.
- [33] T. Yamada, K. Domen, Development of sunlight driven water splitting devices towards future artificial photosynthetic industry, *ChemEngineering* 2 (2018) 36, <https://doi.org/10.3390/chemengineering2030036>.
- [34] R.M. de Vos, H. Verweij, High-selectivity, high-flux silica membranes for gas separation, *Science* 279 (1998) 1710–1711, <https://doi.org/10.1126/science.279.5357.1710>.
- [35] Y. Iwamoto, K. Sato, T. Kato, T. Inada, Y. Kubo, A hydrogen-permselective amorphous silica membrane derived from polysilazane, *J. Eur. Ceram. Soc.* 25 (2005) 257–264, <https://doi.org/10.1016/j.jeurceramsoc.2004.08.007>.
- [36] A.K. Prabhu, S.T. Oyama, Highly hydrogen selective ceramic membranes: application to the transformation of greenhouse gases, *J. Memb. Sci.* 176 (2000) 233–248, [https://doi.org/10.1016/S0376-7388\(00\)00448-8](https://doi.org/10.1016/S0376-7388(00)00448-8).
- [37] T. Yoshioka, M. Kanazashi, T. Tsuru, Micropore size estimation on gas separation membranes: a study in experimental and molecular dynamics, *AIChE J.* 59 (2013) 2179–2194, <https://doi.org/10.1002/aic.13966>.
- [38] M. Kanazashi, T. Tsuru, Design of amorphous silica network structure for molecular sieving membranes and evaluation of pore size by normalized Knudsen-based permeance (NKP), *Zeolite* 35 (2018) 13–22, <https://doi.org/10.20731/zeoraito.35.1.13>.
- [39] S.T. Oyama, D. Lee, P. Hacarlioglu, R.F. Saraf, Theory of hydrogen permeability in nonporous silica membranes, *J. Memb. Sci.* 244 (2004) 45–53, <https://doi.org/10.1016/j.memsci.2004.06.046>.
- [40] S.T. Oyama, M. Yamada, T. Sugawara, A. Takagaki, R. Kikuchi, Review on mechanisms of gas permeation through inorganic membranes, *J. Japan Pet. Inst.* 54 (2011) 298–309, <https://doi.org/10.1627/jpi.54.298>.
- [41] Y. Gu, S.T. Oyama, High molecular permeance in a poreless ceramic membrane, *Adv. Mater.* 19 (2007) 1636–1640, <https://doi.org/10.1002/adma.200602637>.
- [42] S.J. Ahn, G.N. Yun, A. Takagaki, R. Kikuchi, S.T. Oyama, Synthesis and characterization of hydrogen selective silica membranes prepared by chemical vapor deposition of vinyltriethoxysilane, *J. Memb. Sci.* 550 (2018) 1–8, <https://doi.org/10.1016/j.memsci.2017.12.038>.
- [43] P.L. Studt, J.F. Shackelford, R.M. Fulrath, Solubility of gases in glass—a monatomic model, *J. Appl. Phys.* 41 (1970) 2777–2780, <https://doi.org/10.1063/1.1659314>.
- [44] J.S. Masaryk, R.M. Fulrath, Diffusivity of helium in fused silica, *J. Chem. Phys.* 59 (1973) 1198–1202, <https://doi.org/10.1063/1.1680168>.
- [45] R.M. Prasad, Y. Jüttke, H. Richter, I. Voigt, R. Riedel, A. Gurlo, Mechanism of gas separation through amorphous silicon oxycarbide membranes, *Adv. Eng. Mater.* 18 (2016) 721–727, <https://doi.org/10.1002/adem.201500380>.
- [46] D. Lee, L. Zhang, S.T. Oyama, S. Niu, R.F. Saraf, Synthesis, characterization, and gas permeation properties of a hydrogen permeable silica membrane supported on porous alumina, *J. Memb. Sci.* 231 (2004) 117–126, <https://doi.org/10.1016/j.memsci.2003.10.044>.
- [47] Y. Mise, S.J. Ahn, A. Takagaki, R. Kikuchi, S.T. Oyama, Fabrication and evaluation of trimethylmethoxysilane (TMMOS)-derived membranes for gas separation, *Membranes* 9 (2019) 123, <https://doi.org/10.3390/membranes9100123>.
- [48] L.-L. Lee, D.-S. Tsai, A hydrogen-permselective silicon oxycarbide membrane derived from polydimethylsilane, *J. Am. Ceram. Soc.* 82 (1999) 2796–2800, <https://doi.org/10.1111/j.1151-2916.1999.tb02158.x>.
- [49] T. Yoshioka, E. Nakanishi, T. Tsuru, M. Asaeda, Experimental studies of gas permeation through microporous silica membranes, *AIChE J.* 47 (2001) 2052–2063, <https://doi.org/10.1002/aic.690470916>.
- [50] A.B. Shelekhin, A.G. Dixon, Y.H. Ma, Theory of gas diffusion and permeation in inorganic molecular-sieve membranes, *AIChE J.* 41 (1995) 58–67, <https://doi.org/10.1002/aic.690410107>.
- [51] R.S.A. de Lange, K. Keizer, A.J. Burggraaf, Analysis and theory of gas transport in microporous sol-gel derived ceramic membranes, *J. Memb. Sci.* 104 (1995) 81–100, [https://doi.org/10.1016/0376-7388\(95\)00014-4](https://doi.org/10.1016/0376-7388(95)00014-4).
- [52] A.J. Burggraaf, Single gas permeation of thin zeolite (MFI) membranes: theory and analysis of experimental observations, *J. Memb. Sci.* 155 (1999) 45–65, [https://doi.org/10.1016/S0376-7388\(98\)00295-6](https://doi.org/10.1016/S0376-7388(98)00295-6).